Main Mechanical and Thermal Problems of the FTU Tokamak Machine

R. Andreani, L. Bettinali, A. Cecchini, E. Di Pietro, M. Gasparotto,
L. Lovisetto, S. Migliori, A. Pizzuto, M. Roccella
Associazione EURATOM-ENEA sulla Fusione, Centro Ricerche Energia Frascati,
C.P. 65, I-00044 Frascati (Roma), Italy

Abstract

The FTU Tokamak in order to reach the expected performance will have to operate steadily at high magnetic fields. Its magnet and vacuum chamber will undergo very high stresses due to thermal and electromagnetic loads for a large number of shots.

In order to assess the feasibility of these components, numerical codes to compute current, magnetic field and temperature distributions and extensive three dimensional finite element stress analysis have been developed. The main results obtained are illustrated.

1. Introduction

The basic idea in the design of the FTU (Frascati Tokamak Upgrade) machine is to try to reach a range of plasma parameters of great thermonuclear interest with reasonable financial effort [1,2]. In FTU, the good energy confinement properties of a compact Tokamak with a medium high toroidal field: 8T, are combined with the strong plasma heating obtained injecting up to 8 MW of radiofrequency power in the lower hybrid "electron mode".

In order to allow performing the experimental programme foreseen for FTU, the toroidal magnet and the vacuum chamber of the machine must withstand very high stresses for a minimum of 10^4 experimental shots.

2. Machine Parameters and Load Assembly

The main parameters of FTU are:

- Plasma major radius (m)	0.935
- Plasma minor radius (m)	0.31
- Toroidal magnetic field on axis (T)	8
- Plasma current at q = 2.5 (MA)	1.6
- Toroidal field flattop duration (s)	1.5
- Pulse repetition rate	1 pulse every 10 min
- Radiofrequency heating power, 1s flattop at 8 GHz·(MW)	8

The entire load assembly is kept, during operation, at liquid nitrogen temperature: -196 °C, to keep power consumption in the magnet coils and in the poloidal field windings within reasonable limits and to take advantage of the higher mechanical properties of the structural materials (stainless steel and copper) at cryogenic temperature.

The basic mechanical structure of the machine is provided by the monolithic toroidal magnet supporting the vacuum chamber and the poloidal field windings (see Fig. 1). A passive structure formed by two sets of copper conductors is installed between the toroidal field magnet and the vacuum chamber to assist the poloidal field windings in assuring the plasma position control (see Fig. 1).

3. Toroidal Magnet

3.1 Magnet Assembly

The FTU toroidal magnet consists of 12 modules. In each module, two copper coils are enclosed by a stainless steel casing. Each coil has 42 turns obtained from wedge shaped ETP hard drawn copper sheets. Electrical connections between turns are made in the outer region by brazing adjacent plates to form a helyx. Sheets of glass fabric epoxy ~ 0.20 mm thick are used to obtain the inter turn insultation. Casings of the same materials ~ 4 mm thick insulate the coils vs ground. Mechanical continuity of the structure is obtained in the outer region by spacing wedges.

3.2 Magnet Loads

3.2.1 - Electrodynamic loads

The Toroidal Fields Coils are subject to centrifugal body forces due to the interaction of the coil currents (T.F.C.) with the created magnetic field. The distribution of such forces results in a net force towards the torus axis of ~ 5.2 MN per module. The interaction between the T.F.C. and the vertical magnetic field produces a tilting moment of ~ 1 MNm on each module.

3.2.2 - Thermal loads

Owing to the geometry of the turns, the current distribution is affected by a large skin effect. The thermal gradients produced in the plates together with the mean temperature raise result in additional stresses in the whole structure.

3.3 Load Calculations

It has been assumed, for the load calculations, that the magnet is electrically and thermally axisymmetric. Consequently a two-dimensional analysis is sufficient to assess the electrodynamic forces and the temperature distribution. Typical current and temperature distributions, computed by an ad hoc numerical code [3], along the turn minor radius are shown in Fig. 2.

3.4 Stress Analysis

To evaluate the stresses in the overall structure, an extensive three-dimensional F.E. computations has been carried out by means of "BERSAFE" [4] code. It is to be noted that, from a mechanical point of view it was not possible to find a reasonable assumption to reduce the problem to a 2-D one. The whole structure, owing to its modularity, has been studied considering only 1/4 of a module suitably supported. The finite element discretization has been accomplished using cartesian 8 nodes elements. A typical mesh is shown in Fig. 3

Stress computations have been carried out at the most relevant times during the

toroidal field current pulse, i.e. at the end of the current rise (E.C.R.), end of the current flattop (E.C.F.). The results of the computations show the maximum equivalent stress (Von Mises) to be $\cong$ 540 MPa for the stainless steel of the casings and $\cong$ 230 MPa for the copper. The yield stresses at the working temperature are 810 MPa for steel and 300 MPa for copper. For the insulating material, the stress conditions are well characterized by the compressive stress across the thickness and by the tensile strain along the layers of insulator. The corresponding values are σ_r = - 80 MPa and $\varepsilon_t \cong 2.2\times10^{-3}$. An extensive experimental work [5] has shown that the insulating material can withstand safely such loads, for the number of cycles required. Shear stresses in the glass fabric epoxy between turns have been found to be low ($\leq$ 5 MPa). Typical stress and strain distributions are shown in Figs. 4,5.

4. The Vacuum Vessel

The vacuum vessel is a stainless steel structure completely welded, designed in compliance with high vacuum requirements [1,6]. The vacuum vessel has a major radius of 0.935 m and a minor radius of 0.335 m and consists of 12 toroidal thin sectors (see Fig. 6) joined together by thick rigid sectors which incorporate the ports for diagnostics, pumping, auxiliary plasma heating and poloidal limiters. The inner wall of the vacuum chamber has been protected with suitable metallic shields to avoid generating prohibitive thermal stresses. The thickness of the inner wall of the toroidal sectors has been chosen making a reasonable compromise between the mechanical strength and the electrical requirements during the plasma current start-up phase [7]. A 2 mm thickness is a good choice which optimises the mechanical strength without appreciably short circuiting the poloidal flux during the plasma start up. Only 0.12 Vs are lost out of a total of 6.4 Vs.

4.1 Working Temperature and Thermal Wall Loading

The temperature distribution on the vacuum chamber walls, under normal operating conditions, has been evaluated with the following assumptions:

- thermal exchanges by radiation are neglected;
- the vacuum wall is cooled by convection by still nitrogen gas at - 196 °C;
- thermal loads of 130 J/cm^2 per shot have been taken as typical. Thermal load has been derived assuming that 50% of the RF power is directly deposited on 50% of the chamber wall;
- The whole device, at the beginning of the experimental run, is cooled at the liquid nitrogen temperature.

After 5-6 discharges, the vacuum chamber reaches a stationary regime characterized by a maximum surface temperature of the tips of the shields after each shot lower than 500 K and by a temperature difference across the 2 mm thick thermal shield of less than 100 K (see Fig. 7).

In case of a plasma disruption it is assumed that the plasma kinetic energy and the magnetic energy associated with the internal inductance are uniformely deposited on the internal surface of the vacuum vessel. The corresponding power density are respectively 2.8×10^4 W/cm^2 in 0.5 ms and 2.6×10^3 W/cm^2 during 3 ms. The time evolution of the temperature as a function of the shield depth is shown in Fig. 8. It can be noted that the maximum surface temperature occurs after 0.5 ms reaching a value of 1000 K. This variation concerns a material depth of 0.1 mm. After 3.5 ms the temperature has decreased to 400 K while the

thickness of material concerned iS 0.3 mm. In such working condition, thermal cracks will be produced in the stainless steel and consequently thermal shields to protect the vacuum vessel, which has to withstand electromagnetic and pressure loads with a moderate wall thickness, are needed..

4.2 Electromagnetic Loads

The electromagnetic loads on the vacuum vessel are due to the interaction between the induced eddy currents and the magnetic field at the vacuum vessel wall. In the mechanical design of the vacuum vessel, only the stresses produced by a plasma disruption have been considered because this excitation source is a factor between 50 and 100 larger than the others (toroidal magnetic field variations, current variations in the poloidal windings and plasma current variations during normal operation). The plasma disruption has been schematized by a diamagnetic plasma current decay proportional to a poloidal beta variation of 1.8 in 0.5 ms and a toroidal plasma current decay of 1.6 MA in 3 ms. To compute the eddy currents in the vacuum vessel, a numerical method (the network mesh method) [8] has been developed taking into account the presence of the passive copper structure.

The peculiar configuration of the FTU vacuum vessel suggests a subdivision of the surface in rectangular and tee-shaped plates in such a way that the directions of the eddy currents and the current density distribution can be assumed as "a-priori" known. For each plate, the self inductance, the mutuals with the other plates, with the external circuits and with the plasma are evaluated by a numerical code.

The electromagnetic loads are computed considering the interactions between the current induced on each plate and the local magnetic field due to the external circuits, to the copper passive structure, to the plasma and to the currents in the vessel itself. In Figure 9 typical electromagnetic loads are shown in the $\rho.\theta.\phi.$ directions ($\rho.\theta.\phi.$ are the usual quasi-cylindrical coordinate system). These loads are due to the contribution of two components: a symmetric one and an asymmetric one.

4.3 Stress Analysis

To evaluate the stresses in the entire structure, an extensive finite element (F.E.) analysis has been carried out by means of the CASTEM system [9]. The structure has been discretized using 3 nodes shell elements. The simplifying and conservative assumption that all the ports are of tee type has allowed to consider only 1/48 of the entire structure. A typical mesh used and the deformed plot are shown in Fig. 10a e 10b. The vacuum vessel will be constructed using stainless steel type AISI 304 LN having the following properties: Young module 200 GPa, Poisson ratio 0.3; yield strength min 240 MPa and ultimate strength min 550 MPa at room temperature.

The time evolution of the equivalent stress (Von Mises) due to the electrodynamic loads and the atmospheric pressure, acting on the most stressed region of the thin sector is shown in Fig. 11. The maximum value is 246 MPa: 60% of it is due to membrane stress and 40% is due to bending stress. The obtained results show that the stresses acting on the vacuum vessel are acceptable even for few thousand plasma disruptions.

References

[1] "The Frascati Tokamak Upgrade (FTU)" Report 82.49, Associazione EURATOM-ENEA, C.R.E. Frascati (October, 1982).

[2] THE FTU DESIGN TEAM "The FTU Projetc" Proc. of 12th Symposium of Fusion Technology, Jülich, Germany, September 13-17, 1982, pp. 151-160

[3] GIUPPONI, P., RIGHETTI, G.B., "Andamento della Corrente e della Temperatura nell'Avvolgimento Toroidale del Tokamak", Private communication, Frascati (1972).

[4] HELLEN, T.K., FLACK, V., "A User's Guide to BERSAFE Phase II (level 2)", RD/B/N4057, Berkeley Nuclear Laboratories (1977).

[5] BEATRICI, D., BETTINALI, L., RUMI, B., "Tests on the Electrical Insulation of the FTU Tokamak Magnet after Repeated Mechanical Stresses at -193 °C and 23 °C", Proc. of 7th Int. Conf. on Magnet Technology, Karlsruhe, Germany, March 30, April 3, 1981, IEEE Trans. Mag. MAG-17, 5, pp. 2305-2307.

[6] CECCHINI, A., DE FELICE, G., GASPAROTTO, M., RIGHETTI, G.B., "Preliminary Analysis of the Vacuum Vessel and Short-time-constant Copper Shell of the FTU Device", Proc. of 12th Symposium of Fusion Technology, Jülich, Germany, September 13-17, 1982, p. 267-271.

[7] ANDREANI, R., CECCHINI, A., GASPAROTTO, M., LOVISETTO, L., MIGLIORI, S., PIZZUTO, A., "The Vacuum Vessel for the FTU Device: Design Constraints and Stress Analysis" 13th Symposium on Fusion Technology, Varese, Italy, September 24-28, 1984.

[8] GASPAROTTO, M., RIGHETTI, G.M., ROCCELLA, M., "The Vacuum Vessel and Copper Shell Electromagnetic Loads Calculations", 13th Symposium on Fusion Technology, Varese, Italy, September, 24-28, 1984.

[9] Massan, J.C., PASQUET, P., BUNG, H., "CASTEM", Report TC 65.1 CISI Paris

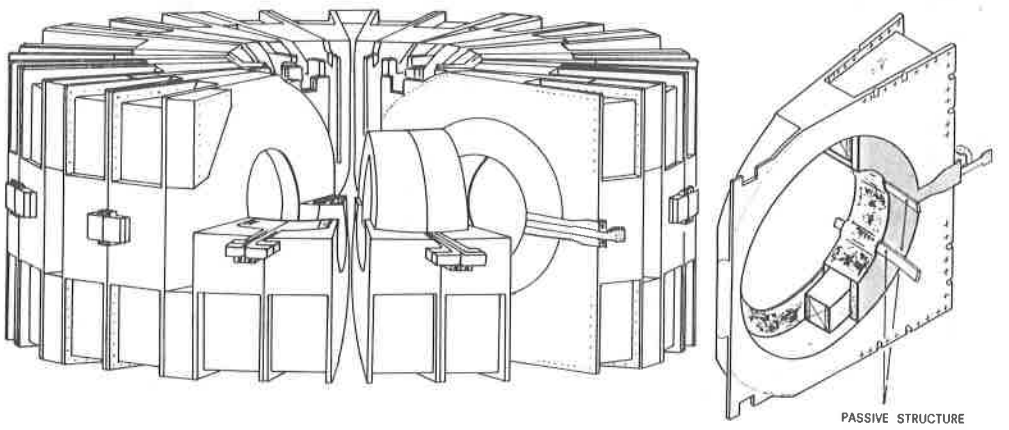

Fig. 1 Toroidal Magnet

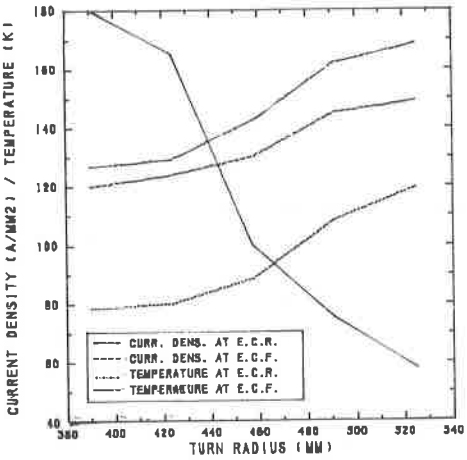

Fig. 2 Current and temperature distribution along the turn minor radius at the inner region

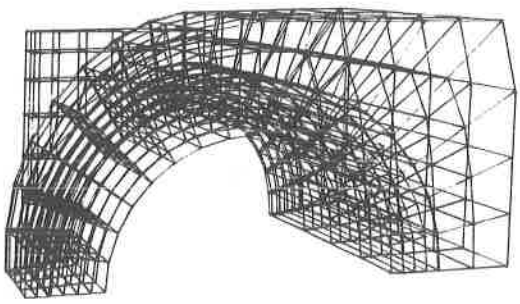

Fig. 3 Magnet-Mesh

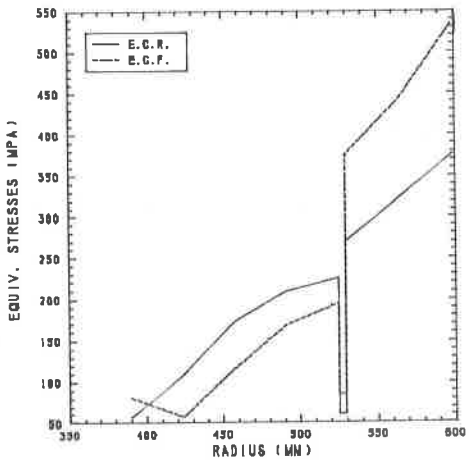

Fig. 4 Equivalent stresses along the Module radius at the inner region

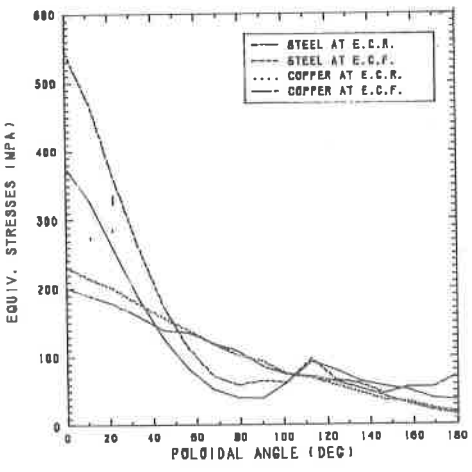

Fig. 5 Equivalent stresses along the poloidal outer profile

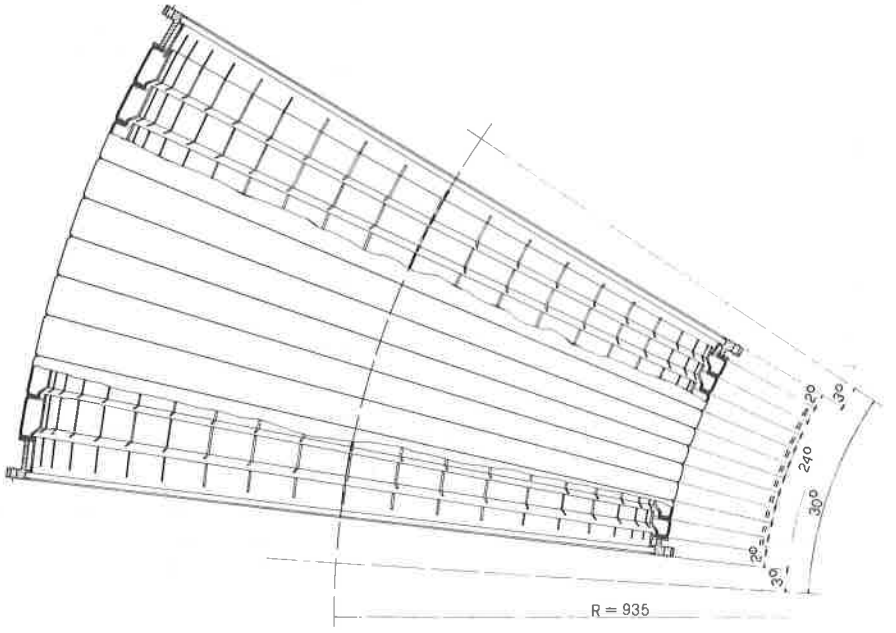

Fig. 6 Vacuum Vessel: toroidal sector

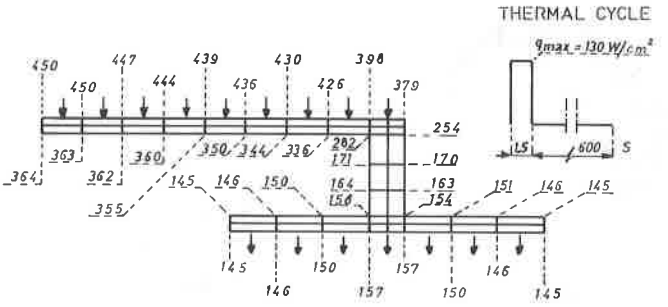

Fig. 7 Temperature distribution during normal operation

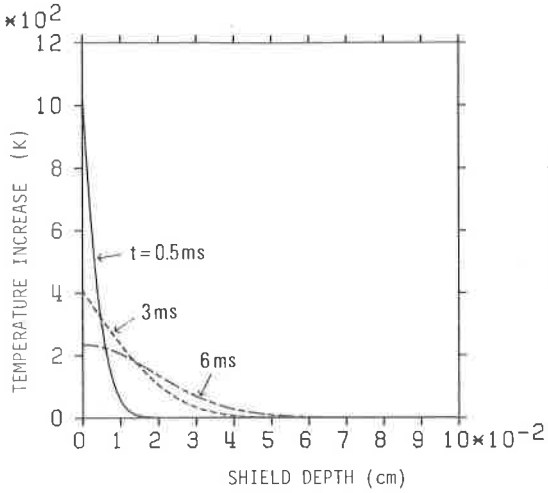

Fig. 8 Temperature distribution in the thermal shields during a plasma disruption

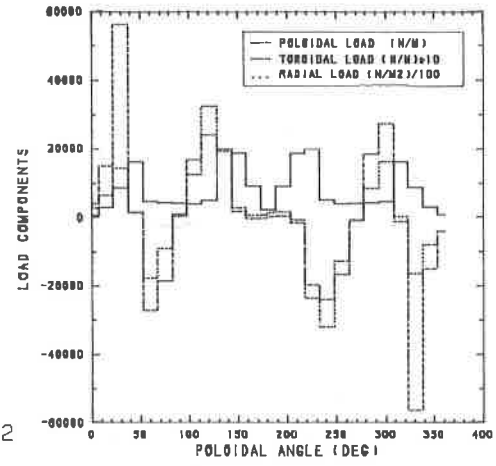

Fig. 9 Electromagnetic loads on the vessel due to the interactions: $J_\theta B_\phi + J_\phi B_\theta$, $J_\theta B_\rho$ and $J_\phi B_\rho$

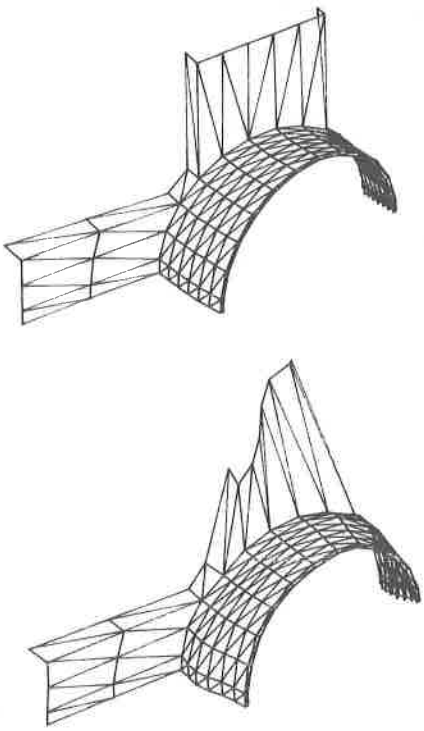

Fig. 10 Mesh and deformed plot of the vacuum vessel

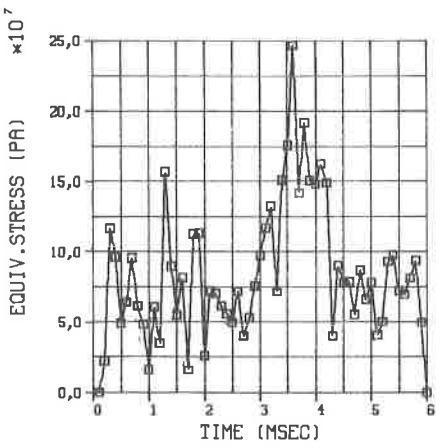

Fig. 11 Von Mises stresses versus time on the most stessed sector region.